

Energy barriers for small electron polaron hopping in bismuth ferrite from first principles

Sabine Körbel*

Institute of Physical Chemistry and Institute of Condensed Matter Theory and Optics, Friedrich Schiller University, Fürstengraben 1, 07743 Jena, Germany

Email Address: skoerbel@uni-muenster.de

Keywords: *polarons, ferroelectrics, domain walls, density-functional theory, electronic transport*

Evidence from first-principles calculations indicates that excess electrons in BiFeO_3 form small polarons with energy levels deep inside the electronic band gap. Hence, n -type electronic transport could occur by hopping of small electron polarons rather than by band-like transport. Here, by means of first-principles calculations, small electron polaron hopping in BiFeO_3 is investigated. Both bulk BiFeO_3 and a typical ferroelectric domain wall, the neutral 71° domain wall, are considered. The latter is included to account for experimental observations of electrical conductivity at domain walls in otherwise insulating ferroelectrics. The object of this study is to shed light on the intrinsic electron conduction in rhombohedral BiFeO_3 and the effect of pristine neutral ferroelectric domain walls. The computed energy barriers for small electron polaron hopping are of the order of the thermal energy at room temperature, both in bulk and within the neutral 71° domain wall. The domain wall is found to act as a two-dimensional trap for small electron polarons with a trap depth of about two to three times the thermal energy at room temperature. Based on these findings, the intrinsic n -type mobility and diffusion constant in BiFeO_3 at room temperature are estimated, and experimental conductivity data for BiFeO_3 are discussed.

1 Introduction

BiFeO_3 may be considered as a ferroelectric version of hematite, Fe_2O_3 . BiFeO_3 is a perovskite with a rhombohedral crystal structure at room temperature, see **Figure 1(a)**, a ferroelectric polarization of $\approx 100 \mu\text{C}/\text{cm}^2$ [1], a bandgap of $\approx 2.7\text{--}3.0$ eV [2, 3, 4, 5, 6, 7, 8], and a magnetic structure close to a collinear G-type antiferromagnet. Like hematite, BiFeO_3 might be suitable for water splitting. Other than hematite, BiFeO_3 is ferroelectric

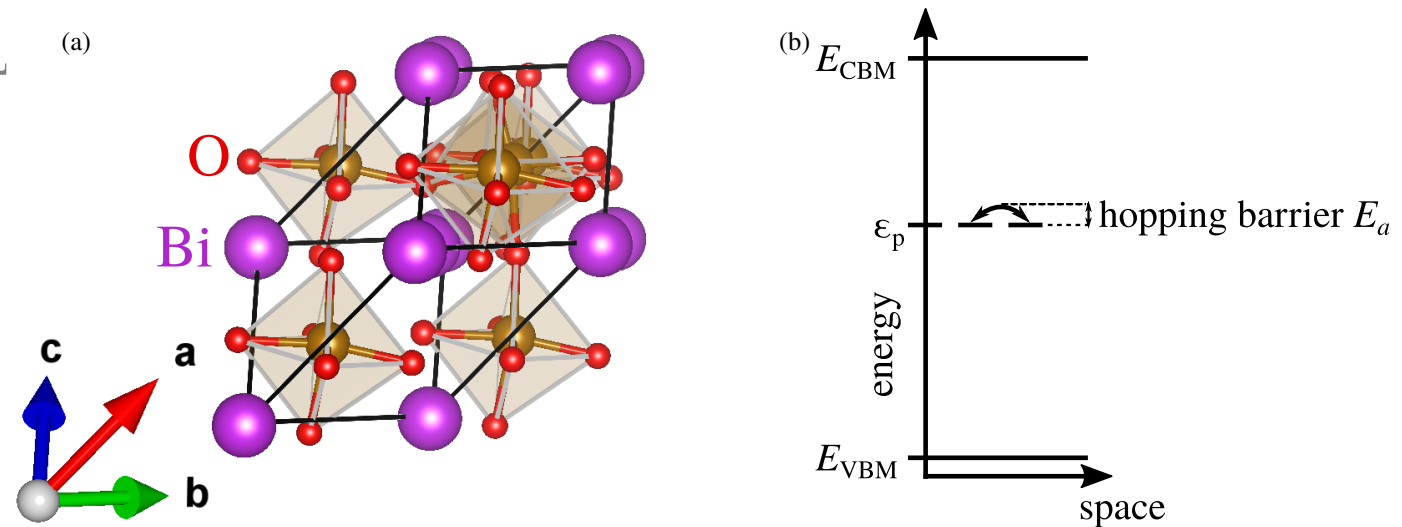


Figure 1: (a) Rhombohedral ($R3c$) unit cell of BiFeO_3 . Because of the antiferromagnetic structure, the unit cell contains two formula units. The ferroelectric polarization is directed along $[111]$. The Fe atoms are surrounded by tilted oxygen octahedra. (b) Schematic band diagram for BiFeO_3 bulk, with valence band maximum (VBM), conduction band minimum (CBM), electron polaron level ε_p , and energy barrier for small electron polaron hopping between neighboring sites. The computed barrier for hopping ($E_a \approx k_B T$ at room temperature) is lower than the energy needed to transfer the electron from the polaron level ε_p to the CBM (≈ 0.7 eV), see section 3.

and can form ferroelectric domain walls, where electronic properties differ from those inside the bulk. In particular, electrical conductivity has been observed at ferroelectric domain walls, whereas the surrounding bulk material is insulating or semiconducting [9, 10, 11, 12, 13, 14]. Like in hematite [15, 16], there is computational evidence that excess electrons in BiFeO_3 form small polarons with energy levels deep inside the band gap [17, 18], and that the small electron polarons are trapped by ferroelectric domain walls [19, 20, 21]. Hence, electronic

transport in n -doped BiFeO_3 could occur by hopping of small electron polarons rather than by band-like transport, and the hopping of electron polarons could require less energy than that needed to promote an electron from the polaron state to the conduction band, see Figure 1(b). Domain walls, if present, could affect electronic transport. Here, first-principles electronic structure calculations based on density-functional theory were performed to determine the energy barriers for electron hopping in the bulk and at one of the prevalent ferroelectric domain walls, the neutral 71° domain wall [22, 23]. The 71° domain wall was chosen because it affects the atomic and electronic structure more strongly than the 109° wall [22, 20], and because it has been reported to be conductive in several studies, such as Ref. [13, 24, 25]. The object of this study is to shed light on the intrinsic n -type conduction mechanism in BiFeO_3 and on the effect of pristine neutral ferroelectric domain walls. The approach taken here allows to determine the intrinsic mechanism of n -type conduction, once excess electrons have been brought into BiFeO_3 in some way. For example, charge carriers may originate from point defects, such as oxygen vacancies or aliovalent dopants or impurities, from photoexcitation resulting in bound or dissociated electron-hole pairs, or from an electrical contact. The approach taken here can predict the intrinsic charge carrier mobility, but it cannot predict the charge-carrier density since the latter depends on the sample fabrication and history and the experimental conditions, and it can hence not predict the absolute electrical conductivity, but it can predict the temperature dependence of the electrical conductivity and the effect of deviations from the perfect crystal structure. External processes of emitting and trapping electrons by defects are not part of the intrinsic electrical conduction mechanism, and considering the effects of all possible defects would be beyond the scope of this work. However, a particular defect (or desired structure modification) is considered here, namely the neutral ferroelectric 71° domain wall.

This paper is organized as follows: First the computational methods are introduced, then the energy barriers for small polaron hopping are presented for bulk and domain wall and the electronic mobility and diffusion constant at room temperature are determined. Finally results are discussed based on experimental data, where available.

2 Methods

The calculations were performed with the program `vasp` [26], using the Projector-Augmented Wave (PAW) method [27, 28] and pseudopotentials with 5 (Bi), 16 (Fe), and 6 (O) valence electrons, respectively. Periodic boundary conditions were employed. The local spin-density approximation (LSDA) to density-functional theory (DFT) was used, and the band gap was corrected with a Hubbard- U of 5.3 eV applied to the Fe- d states using Dudarev's scheme [29]. This approach yields atomic and electronic structure in close agreement with experiment [19, 20, 21]. Standard approaches to model polarons and polaron hopping from first principles are DFT+ U or hybrid DFT functionals, which were applied, e.g., in Ref. [30, 31]. Here, to test how much the calculated hopping barriers depend on the level of theory, the electronic structure with polaron and the polaron hopping barriers in bulk BiFeO_3 obtained with LSDA+ U and with the hybrid HSE functional [32] for the geometries optimized with LSDA+ U are compared. A similar comparison of the hybrid PBE0 functional [33] and DFT+ U and a piecewise linear DFT functional was made in Ref. [34] for polarons in Ga_2O_3 , with the result that polaron formation energy and eigenvalue from DFT+ U and PBE0 agree at least semiquantitatively. Plane-wave basis functions with energies up to 520 eV were used. Both the atomic positions and the cell parameters were optimized until the total energy differences between consecutive iteration steps fell below 0.01 meV for the optimization of the electronic density and below 0.1 meV for the optimization of the atomic structure. BiFeO_3 with excess electrons was modeled using supercells that comprise eight (bulk) or 16 (domain wall) 10-atom unit cells, respectively. Convergence of energy barriers with respect to supercell size was confirmed for bulk, see Supporting Information. One excess electron was added to the supercell, whose charge was compensated by a uniform background charge density. The magnetic structure of BiFeO_3 was approximated by that of a collinear G -type antiferromagnet, spin-orbit coupling was neglected.

2.1 Excess electrons in bulk

BiFeO_3 bulk with excess electrons was modeled using supercells with 80 atoms that consist of $2 \times 2 \times 2$ rhombohedral 10-atom unit cells. The first Brillouin zone of the supercell was sampled with $2 \times 2 \times 2$ k -points, equivalent

to $4 \times 4 \times 4$ k -points for the primitive rhombohedral ten-atom unit cell of BiFeO_3 and to $5 \times 5 \times 5$ k -points for a pseudocubic five-atom perovskite cell with about four Å edge length, as depicted in **Figure 2(a)**.

2.2 Excess electrons at the ferroelectric 71° domain wall

Excess electrons at 71° domain walls were modeled using a 160-atom supercell, see **Figure 2(b)**, spanned by $4(\mathbf{a}_{\text{pc}} + \mathbf{b}_{\text{pc}})$ ($[110]$ in the pseudocubic system, here “ s ”), $(-\mathbf{a}_{\text{pc}} + \mathbf{b}_{\text{pc}} + 2\mathbf{c}_{\text{pc}})$ ($[\bar{1}12]$ in the pseudocubic system), and $(\mathbf{a}_{\text{pc}} - \mathbf{b}_{\text{pc}} + 2\mathbf{c}_{\text{pc}})$ ($[1\bar{1}2]$ in the pseudocubic system), where \mathbf{a}_{pc} , \mathbf{b}_{pc} , and \mathbf{c}_{pc} span the pseudocubic 5-atom cell. This supercell is based on that used in Ref. [19, 20, 21]. The atomic structures and formation energies of low-energy ferroelectric domain walls in BiFeO_3 are well known [35, 22, 36, 23, 37]. Atomic and electronic structure of the neutral 71° domain wall investigated here have been published elsewhere [23, 22, 19, 20, 21]. The antiferromagnetic G -type spin configuration of the bulk was maintained in the systems with domain walls. The first Brillouin zone of the supercell was sampled with $1 \times 3 \times 3$ k -points, equivalent to $5 \times 5 \times 5$ k -points for the primitive rhombohedral ten-atom unit cell of BiFeO_3 and to $7 \times 7 \times 7$ k -points for a pseudocubic five-atom perovskite cell with about four Å edge length.

2.3 Polaron hopping

According to previous works [17, 18, 19, 20, 21], the excess electron localizes mostly on a single Fe site. In bulk BiFeO_3 , all Fe sites are equivalent. Localization on a specific Fe site was induced by means of the occupation matrix control (OMC) method of Allen and Watson [38].

Energy barriers for polaron hopping between different Fe sites were obtained using the nudged-elastic-band (NEB) method, in which an artificial spring force acting along the hopping path constrains atomic structure optimization to directions perpendicular to the path. Nine configurations (NEB images) along each hopping path were considered, including initial and final state.

Both hops between nearest-neighbor (NN) and second-nearest neighbor (2NN) Fe sites were considered, since NN hops require spin flip of the electron and should hence be suppressed.

The number of inequivalent NN and 2NN hops is limited by symmetry. In bulk, there is one NN hop and two inequivalent 2NN hops: a 2NN hop perpendicular to the ferroelectric polarization direction, and a 2NN hop in a direction that forms an angle of $\alpha \approx 35^\circ$ with the polarization direction, see **Figure 2(a)**. At ferroelectric domain walls, Fe sites are still equivalent within planes parallel to the wall, but differ between these planes. Hops can occur along the wall or with a component perpendicular to the wall, see **Figure 2(b)**. NEB calculations were considered converged when the energy barrier changed by maximally 1 meV in two consecutive iterations of the NEB structure optimization. The strain dependence of the barriers was also investigated. The strain reference (zero strain, $\varepsilon = 0$) corresponds to the optimized geometry of bulk or domain wall without excess electron. Tensile strain, $\varepsilon > 0$, corresponds to the optimized geometry of bulk or domain wall with excess electron.

2.4 Transition state theory

The abrupt jump of the small electron polaron from initial to final site (see below) as a function of the hopping coordinate indicates that the hopping process is non-adiabatic rather than adiabatic. Marcus theory [39] was applied to obtain non-adiabatic hopping rates of small electron polarons between 2NN lattice sites in BiFeO_3 . NN hopping, being spin-forbidden, was neglected. The transition rate k is then

$$k = \frac{2\pi}{\hbar} |\langle \psi_i | H | \psi_f \rangle|^2 \frac{1}{\sqrt{4\pi\lambda k_B T}} \exp\left(-\frac{E_a}{k_B T}\right). \quad (1)$$

E_a is the activation energy (hopping barrier) for the 2NN hop, λ is the reorganization energy. For symmetric hops, $\lambda = 4E_a$. The electronic coupling matrix elements $\langle \psi_i | H_c | \psi_f \rangle$, where the $\psi_{i,f}$ are electronic wave functions localized on the initial and final Fe site, respectively, were adopted from Ref. [40], where they were calculated for $\text{Fe}(\text{H}_2\text{O})_6^{5+}$ complexes as a function of the Fe-Fe distance from a model Hamiltonian that treated Fe with a pseudopotential and H_2O as classical point charges. Here, the matrix element for the second-nearest Fe-Fe distance calculated for bulk BiFeO_3 , 5.516 Å, was used throughout ($-101.875 \text{ cm}^{-1} \approx -0.013 \text{ eV}$). Alternatively,

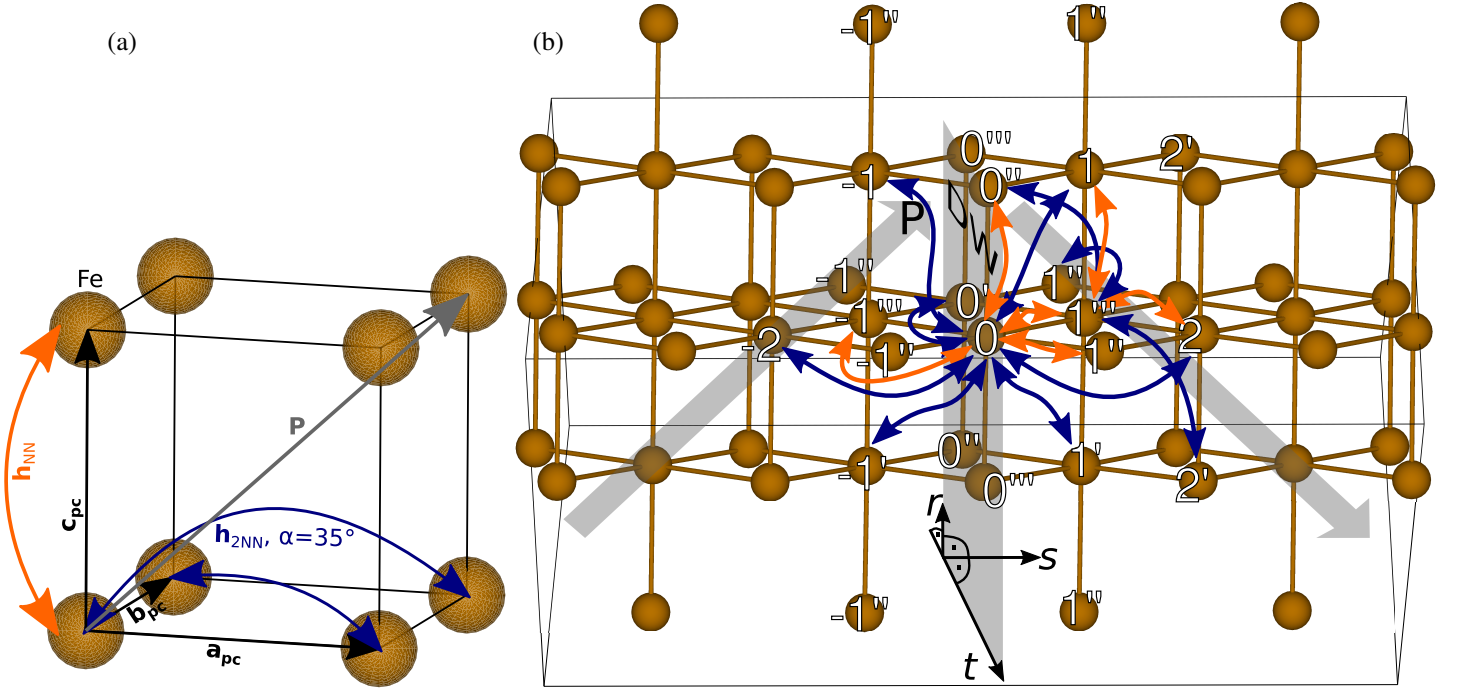


Figure 2: (a) Fe network (schematic) and hops \mathbf{h} between nearest neighbors (NN, orange) and second-nearest neighbors (2NN, dark-blue) in bulk BiFeO₃. For clarity, only Fe atoms are shown. There is one irreducible hop between nearest neighbors and two inequivalent hops between second-nearest neighbors that form an angle with the ferroelectric polarization \mathbf{P} of $\alpha \approx 90^\circ$ and $\alpha \approx 35^\circ$, respectively. (b) 160-atom supercell with the 71° domain wall (DW) and hopping paths considered. The coordinates s , r , and t are orthogonal. r and t span the domain-wall plane, s is perpendicular to the domain wall, t is perpendicular to the polarization \mathbf{P} .

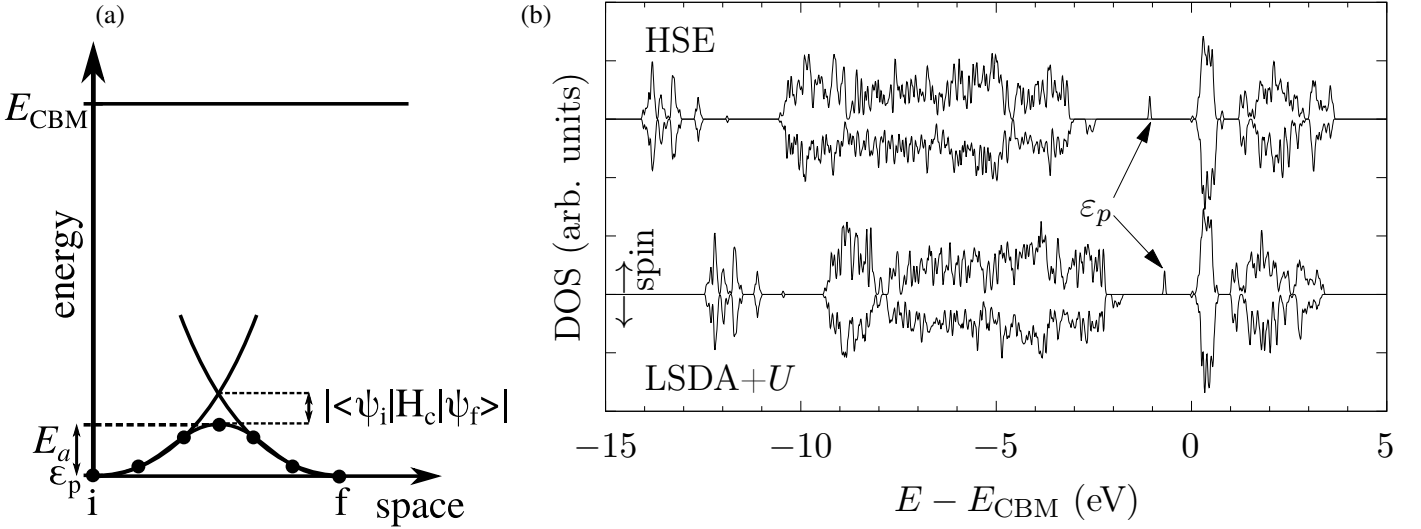


Figure 3: (a) Extracting the coupling matrix element $\langle \psi_i | H_c | \psi_f \rangle$ between initial state (i) and final state (f) from the hopping energy profile. (b) Electronic density of states with electron polaron from LSDA+U and HSE. The energy of the conduction band minimum (CBM) is set to zero. ϵ_p is the computed polaron level.

the coupling matrix elements could be determined as the deviation of the calculated barrier from the parabolic crossing point, see **Figure 3(a)**. In the case of compressive strain, where the calculated hopping energy profile is close to a double parabola, one obtains a coupling matrix element of $\langle \psi_i | H_c | \psi_f \rangle \approx -2$ to -3 meV.

The electron mobility μ_e and the diffusion constant D are obtained from the transition rate k using the Einstein relation as

$$\mu_e = \frac{De}{k_B T} = \frac{e |\mathbf{h}|^2 n_f k}{2 d k_B T}, \quad (2)$$

where e is the elementary charge, $|\mathbf{h}|$ is the hopping distance, n_f is the number of equivalent available final states for a given initial state, d is the dimension, k_B is Boltzmann's constant, and T is the temperature, here 300 K. For bulk, $d=3$, $n_f^{\text{bulk}}=12$ for 2NN hops, $|\mathbf{h}| = \sqrt{2}a_0$ is the 2NN Fe-Fe distance, and a_0 the pseudocubic lattice constant (about 4 Å). For two-dimensional transport within a domain-wall plane, $d = 2$. Hops along the r coordinate consist of two consecutive hops, such as $0''' \rightarrow 1''' \rightarrow 0''$, with $|\mathbf{h}_r| = 2a_0$ and $n_{f,r} = 4$. Hops along the t coordinate can be single 2NN hops with $|\mathbf{h}_t| = \sqrt{2}a_0$ and $n_{f,t}=2$, such as $0 \rightarrow 0'$, or double 2NN hops with $n_{f,t2} = 4$ and $|\mathbf{h}_t| = \sqrt{2}a_0$, such as $0' \rightarrow 1 \rightarrow 0$. The effective barrier for double hops was taken as the higher one of the two. The two-dimensional n -type mobility and the diffusion constant in the domain wall are computed as

$$\mu_e^{\text{DW}} = \frac{e D^{\text{DW}}}{k_B T} = \frac{e}{4 k_B T} \left(k_r^{\text{eff}} |\mathbf{h}_r|^2 n_{f,r} + k_{t1}^{\text{eff}} |\mathbf{h}_t|^2 n_{f,t1} + k_{t2}^{\text{eff}} |\mathbf{h}_t|^2 n_{f,t2} \right). \quad (3)$$

3 Results

3.1 Excess electrons in bulk

Electronic structure from LSDA+U and HSE:

The electronic density of states (DOS) for a supercell (80 atoms) with an electron polaron is shown in Figure 3(b). The DOS obtained with LSDA+U and HSE agree semiquantitatively. The computed polaron level ε_p lies 0.7 eV below the conduction band minimum for LSDA+U and 1 eV below the conduction band minimum for HSE, with an estimated uncertainty of 0.2 eV.

Hopping barriers:

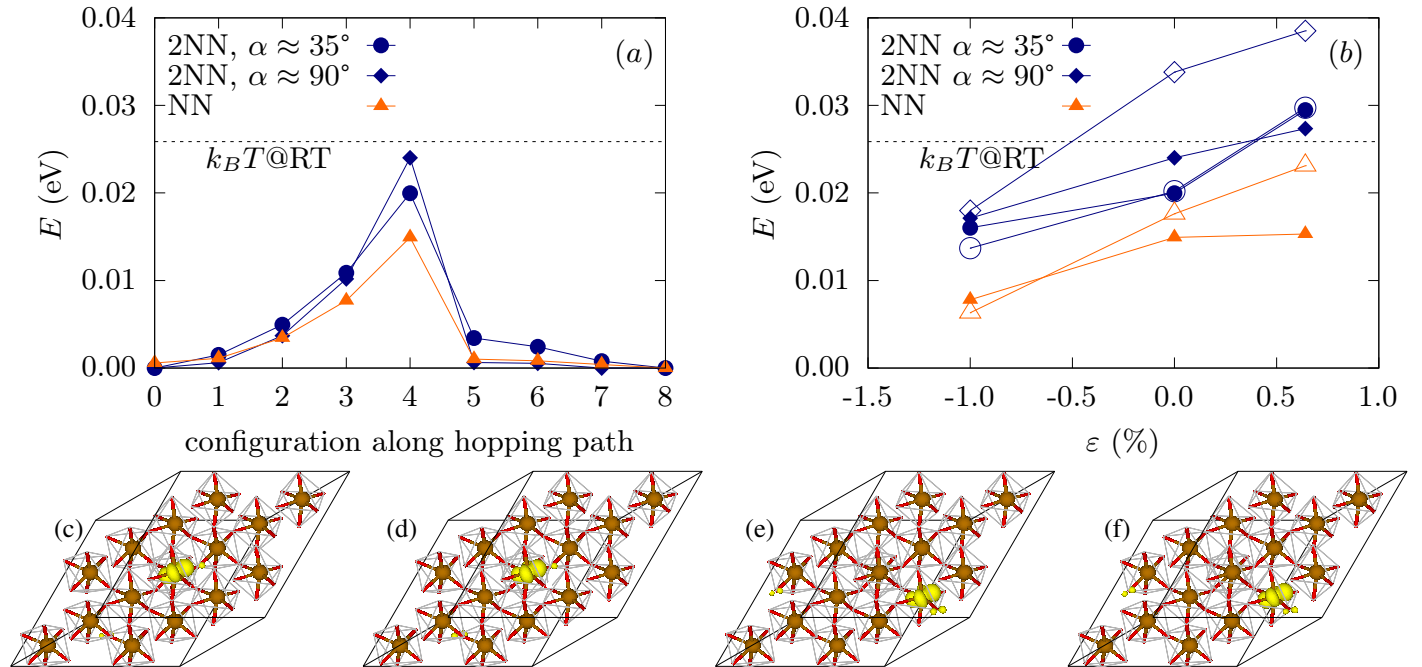


Figure 4: (a) Energy profile of first- (orange triangles) and second-nearest neighbor hops (dark-blue circles and diamonds) in bulk for zero strain along the hopping path. The configurations 0 and 8 belong to initial and final state, respectively. (b) Hopping barriers of NN and 2NN hops as a function of strain ε . The lines are a guide to the eye. Solid symbols: LSDA+U, empty symbols: HSE. (c) to (f): isosurface of the density of the excess electron (yellow; isosurface level: $\approx 2\%$ of the maximum) of configuration 0, 4, 5, and 8 of the 2NN hop with $\varepsilon = 0$ and $\alpha \approx 90^\circ$. Fe atoms are shown as brown spheres.

The energy barriers for NN hops and the two different 2NN hops are depicted in **Figure 4(a)** and **(b)** for different strains ε . Both NN and 2NN barriers are of the order of the thermal energy at room temperature and shrink upon compression. Hence, the hopping barrier is an order of magnitude smaller than the energy distance to the conduction band minimum. The 2NN barriers are not strongly direction dependent. The transitions from initial to

Table 1: Computed energy barrier E_a in meV for small electron hopping in bulk BiFeO₃ from LSDA+ U and from HSE for different strains. 0.64% strain corresponds to \approx the experimental cell volume at room temperature. The estimated uncertainty is \approx 10 meV.

ε	NN		2NN, $\alpha \approx 90^\circ$		2NN, $\alpha \approx 35^\circ$	
	LSDA+ U	HSE	LSDA+ U	HSE	LSDA+ U	HSE
-1.0%	8	6	17	18	16	14
0	15	18	24	34	20	20
0.64%	15	25	27	39	29	30

Table 2: Computed 2NN energy barrier E_a in meV for small electron hopping in different directions at 71° domain walls (DW) in BiFeO₃ for different strains and extrapolated to the experimental cell volume at room temperature. The estimated uncertainty is \approx 10 meV. The extrapolated barriers were used to calculate the mobility and diffusion constant with Eq. (3).

ε	double 2NN, r or $t2$	2NN, $t1$	2NN, escape from DW
-0.17%	31	16	57
0	32	25	62
0.34%	33	27	65
0.65% (extrapol.)	35	29	67

final site are non-adiabatic (abrupt), as seen from the isosurface of the excess electron’s density as a function of the hopping coordinate (yellow orbitals in Figure 4(c)–(f)). The computed energy barriers are listed in Table 1. To obtain the electron mobility and the diffusion constant at room temperature, the barrier at $\varepsilon \approx 0.65\%$, corresponding to the experimental lattice constant at room temperature [41], was used. With an energy barrier of 28 meV (the average of the two 2NN barriers) and a hopping distance of the 2NN Fe-Fe distance, the computed electron mobility in BiFeO₃ bulk at room temperature is $\mu_e^{\text{bulk}} \approx 0.6 \text{ cm}^2/\text{Vs}$, the computed diffusion constant is $D \approx 0.02 \text{ cm}^2/\text{s}$. The uncertainty of the computed μ_e and D are about one order of magnitude.

3.2 Excess electrons at domain walls

When starting from a delocalized-electron configuration, a small electron polaron forms spontaneously in the plane labeled “1” (on the right-hand side of the wall, if the net polarization points to the right, see Figure 2(b)), which is a metastable site. The most stable site is inside the domain wall, in the plane labeled “0”. **Figure 5** shows the energy barriers for electron hops at the 71° domain wall. Only the lowest barriers in each direction are shown. All barriers are depicted and tabulated in the Supplemental Information. The hops are projected on the symmetry-adapted coordinates (see Figure 5) s [\perp wall, (a)], r [within the wall, (b)], and t [within the wall, $\perp \mathbf{P}$, (c)]. For hops between the two trap states in the planes “0” and “1”, the barrier [bright symbols and lines in (a)] is similar to the thermal energy at room temperature, whereas for hops out of the wall (from plane “0” or “1” to plane “-1”, “2”, or “-2”) the barrier is about 2–3 times larger. For hops within the domain wall [(b) and (c)] there are paths available with barriers similar to the thermal energy at room temperature. Barriers are invariant with respect to translation by a lattice vector parallel to the wall. Like in bulk, the barriers shrink upon compression. The lowest barriers for NN and 2NN hops are similar in size. The computed 2NN energy barriers are listed in Table 2 and in the Supporting Information.

The computed two-dimensional electron mobility inside the domain-wall plane is $\mu_e^{\text{DW}} \approx 0.8 \text{ cm}^2/\text{Vs}$, the computed two-dimensional diffusion constant inside the domain wall is $D \approx 0.02 \text{ cm}^2/\text{s}$. μ_e and D have an uncertainty of about one order of magnitude.

4 Discussion

Hall measurements for hematite resulted in electron mobilities of about 0.01 to $>1 \text{ cm}^2/\text{Vs}$ [42, 43, 44], near the upper end of which lies the here computed mobility in bulk BiFeO₃ of $0.6 \text{ cm}^2/\text{Vs}$. Given the similarities in atomic and electronic structure of BiFeO₃ and hematite, it seems plausible that intrinsic mobilities of BiFeO₃ and hematite should be comparable.

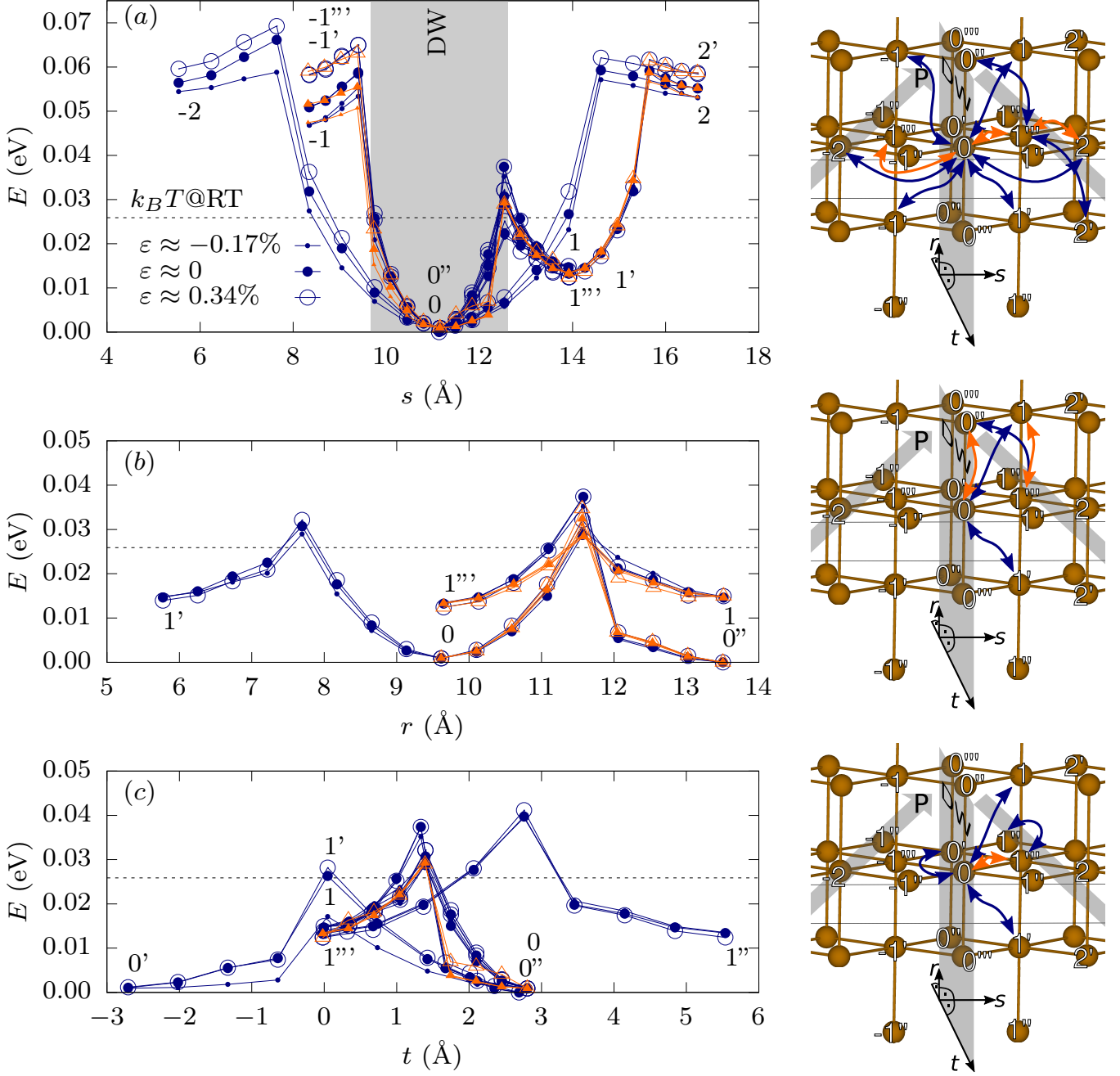


Figure 5: Energy barriers of polaron hops at the 71° domain wall. (a) All hops with a component across the wall, (b) and (c): selected hops with components along the wall. Orange triangles: nearest-neighbor, dark-blue circles: second-nearest-neighbor hops. Numbers indicate the Fe positions in Figure 2(b). Hop directions were projected on (a) the s coordinate, (b) the r coordinate, and (c) the t coordinate, see Figure 2(b).

Experimentally determined activation energies of electron conduction in BiFeO_3 are typically much larger (between about 0.1 and 1.3 eV [45, 46, 47, 48, 49]) than the here computed barrier of about 28 meV, indicating that the experimentally determined barriers do not originate from electron polaron hopping in pristine bulk nor from escape of electron polarons from pristine neutral ferroelectric domain walls, assuming that the other typical walls, the 109° and the 180° walls, exhibit a similar or smaller trap depth than the 71° wall. It seems likely that the experimentally determined barriers of several hundred meV originate from defects other than pristine neutral ferroelectric domain walls, for example from point defects, such as oxygen or bismuth vacancies, or from interface effects, such as Schottky barriers. In Refs. [13, 50] an activation barrier of ≈ 0.7 eV was found for n -type conduction, which is about the energy difference between the electron polaron level and the conduction band minimum computed here. In principle, this activation barrier of 0.7 eV could originate from emission of

electrons from the polaron state to the conduction band. This would mean that transport by emission from polarons into delocalized conduction states and subsequent ballistic transport would be more efficient than polaron hopping, inspite of the much higher energy barrier that must initially be overcome. However, there are reasons to believe that the lifetime of thermalized electrons in the conduction band at room temperature should be small. This is because the strong Fe-*d* contribution to the states at the conduction band minimum and the small size of the electron polaron indicate that electron-phonon coupling should be large, which should lead to strong electron-phonon scattering. First-principles molecular dynamics simulations yield a polaron formation time of less than a picosecond [20]. Once a small electron polaron has formed, it is unlikely to transform into a delocalized conduction-band electron at room temperature since the energy distance between the polaron level and the conduction-band minimum of $|\epsilon_p| \approx 0.7$ eV is much larger than the polaron hopping barrier of $E_a \approx 30$ meV. It seems most likely that at least for thermalized electrons at temperatures \lesssim room temperature, small electron hopping should be the dominant intrinsic *n*-type transport process, and that in the reported experimental measurements of the electrical conductivity, the small barrier of ≈ 30 meV for electron polaron hopping is hidden behind much larger barriers associated with emission from defects or interfaces other than pristine neutral ferroelectric domain walls.

5 Summary and conclusion

Energy barriers for small electron polaron hopping in BiFeO₃ were determined using density-functional theory. Hopping in perfect, pristine BiFeO₃ and at pristine, neutral ferroelectric 71° domain walls was considered. In both bulk and domain-wall plane, the calculated energy barriers are of the order of $k_B T$ at room temperature ($\approx 15 - -40 \pm 10$ meV) and are reduced by compressive strain. Using non-adiabatic Marcus theory, an electron mobility of $\mu_e^{\text{bulk}} \approx 0.6$ cm²/Vs and $\mu_e^{\text{DW}} \approx 0.8$ cm²/Vs for bulk and within the domain-wall plane, respectively, is obtained at room temperature. The computed diffusion constant in bulk at room temperature is $D \approx 0.02$ cm²/s both in the bulk and in the domain-wall planes. μ_e and D have an uncertainty of about one order of magnitude. The domain wall planes act as traps for small electron polarons, with a trap depth of about two to three times $k_B T$ at room temperature ($\approx 70 \pm 10$ meV). These findings indicate that (a) the effect of pristine, neutral ferroelectric domain walls on the *n*-type conductivity at room temperature consists in accumulating excess electrons and confining their motion to the domain-wall plane. In the Drude picture (conductivity \sim carrier density \times mobility), the electron density along the wall is enhanced compared to the bulk, the mobility perpendicular to the wall is reduced compared to bulk. This is in line with experimental observations that conductivity is enhanced at ferroelectric domain walls and in directions parallel to the domain walls, (b) experimentally found activation barriers of several hundred meV for electrical conductivity in BiFeO₃ should have an origin other than electron polaron hopping in pristine BiFeO₃ or electron polaron escape from pristine neutral ferroelectric 71° domain walls.

Supporting Information

Supporting Information is available from the Wiley Online Library or from the author.

Acknowledgements

S. K. thanks Michele Reticcioli for recommending the OMC method. This project has received funding from a postdoc stipend of the University of Jena, Germany and from the Volkswagen Stiftung (Momentum) through the project “dandelion”. Computational resources and support were supplied by the HPC cluster ARA of the University of Jena, Germany. Figures were made using VESTA [51] and gnuplot.

References

- [1] D. Lebeugle, D. Colson, A. Forget, M. Viret, *Appl. Phys. Lett.* **2007**, *91*, 2 022907.
- [2] S. R. Basu, L. W. Martin, Y. H. Chu, M. Gajek, R. Ramesh, R. C. Rai, X. Xu, , J. L. Musfeldt, *Appl. Phys. Lett.* **2008**, *92*, 9 091905.
- [3] A. J. Hauser, J. Zhang, L. Mier, R. A. Ricciardo, P. M. Woodward, T. L. Gustafson, L. J. Brillson, F. Y. Yang, *Appl. Phys. Lett.* **2008**, *92*, 22 222901.

- [4] J. Ihlefeld, N. Podraza, Z. Liu, R. Rai, X. Xu, T. Heeg, Y. Chen, J. Li, R. Collins, J. Musfeldt, et al., *Appl. Phys. Lett.* **2008**, 92, 14 142908.
- [5] A. Kumar, R. C. Rai, N. J. Podraza, S. Denev, M. Ramirez, Y.-H. Chu, L. W. Martin, J. Ihlefeld, T. Heeg, J. Schubert, et al., *Appl. Phys. Lett.* **2008**, 92, 12 121915.
- [6] V. Železný, D. Chvostová, L. Pajasová, I. Vrejoiu, M. Alexe, *Applied Physics A* **2010**, 100, 4 1217.
- [7] D. Sando, C. Carrétéro, M. N. Grisolia, A. Barthélémy, V. Nagarajan, M. Bibes, *Advanced Optical Materials* **2018**, 6, 2 1700836.
- [8] R. Moubah, G. Schmerber, O. Rousseau, D. Colson, M. Viret, *Applied Physics Express* **2012**, 5, 3 035802.
- [9] J. Seidel, L. W. Martin, Q. He, Q. Zhan, Y.-H. Chu, A. Rother, M. Hawkrigde, P. Maksymovych, P. Yu, M. Gajek, et al., *Nat. Mater.* **2009**, 8, 3 229.
- [10] A. Bhatnagar, A. R. Chaudhuri, Y. H. Kim, D. Hesse, M. Alexe, *Nature communications* **2013**, 4 2835.
- [11] J. Guyonnet, I. Gaponenko, S. Gariglio, P. Paruch, *Advanced Materials* **2011**, 23, 45 5377.
- [12] T. Rojac, A. Bencan, G. Drazic, N. Sakamoto, H. Ursic, B. Jancar, G. Tavcar, M. Makarovic, J. Walker, B. Malic, et al., *Nat. Mater.* **2017**, 16, 3 322.
- [13] S. Farokhipoor, B. Noheda, *Phys. Rev. Lett.* **2011**, 107, 12 127601.
- [14] F. Risch, Y. Tikhonov, I. Lukyanchuk, A. M. Ionescu, I. Stolichnov, *Nature Communications* **2022**, 13 7239.
- [15] C. Lohaus, A. Klein, W. Jaegermann, *Nat. Commun.* **2018**, 9, 1 1.
- [16] H. Peng, S. Lany, *Phys. Rev. B* **2012**, 85, 20 201202R.
- [17] Geneste, Grégory and Paillard, Charles and Dkhil, Brahim, *Phys. Rev. B* **2019**, 99 024104.
- [18] A. Radmilovic, T. J. Smart, Y. Ping, K.-S. Choi, *Chem. Mater.* **2020**, 32, 7 3262.
- [19] S. Körbel, J. Hlinka, S. Sanvito, *Phys. Rev. B* **2018**, 98 100104(R).
- [20] S. Körbel, S. Sanvito, *Phys. Rev. B* **2020**, 102 081304(R).
- [21] S. Körbel, *Phys. Rev. Materials* **2023**, 7, 10 104402.
- [22] Diéguez, Oswaldo and Aguado-Puente, Pablo and Junquera, Javier and Íñiguez, Jorge, *Phys. Rev. B* **2013**, 87 024102.
- [23] Y. Wang, C. Nelson, A. Melville, B. Winchester, S. Shang, Z.-K. Liu, D. G. Schlom, X. Pan, L.-Q. Chen, *Phys. Rev. Lett.* **2013**, 110, 26 267601.
- [24] Y.-P. Chiu, Y.-T. Chen, B.-C. Huang, M.-C. Shih, J.-C. Yang, Q. He, C.-W. Liang, J. Seidel, Y.-C. Chen, R. Ramesh, et al., *Advanced Materials* **2011**, 23, 13 1530.
- [25] Y. Zhang, H. Lu, X. Yan, X. Cheng, L. Xie, T. Aoki, L. Li, C. Heikes, S. P. Lau, D. G. Schlom, L. Chen, A. Gruverman, X. Pan, *Advanced Materials* **31**, 36 1902099.
- [26] G. Kresse, J. Furthmüller, *Comput. Mater. Sci.* **1996**, 6, 1 15.
- [27] P. E. Blöchl, *Phys. Rev. B* **1994**, 50 17953.
- [28] G. Kresse, D. Joubert, *Phys. Rev. B* **1999**, 59 1758.
- [29] S. L. Dudarev, G. A. Botton, S. Y. Savrasov, C. J. Humphreys, A. P. Sutton, *Phys. Rev. B* **1998**, 57 1505.

- [30] M. Setvin, C. Franchini, X. Hao, M. Schmid, A. Janotti, M. Kaltak, C. G. Van de Walle, G. Kresse, U. Diebold, *Phys. Rev. Lett.* **2014**, *113*, 8 086402.
- [31] E. Ghorbani, L. Vill, P. Erhart, A. Klein, , K. Albe, *Phys. Rev. Materials* **2022**, *6* 074410.
- [32] J. Heyd, G. E. Scuseria, M. Ernzerhof, *J. Chem. Phys.* **2003**, *118*, 18 8207.
- [33] C. Adamo, V. Barone, *J. Chem. Phys.* **1999**, *110* 6158.
- [34] S. Falletta, A. Pasquarello, *Phys. Rev. B* **2023**, *107* 205125.
- [35] J. Fousek, V. Janovec, *J. Appl. Phys.* **1969**, *40*, 1 135.
- [36] W. Ren, Y. Yang, O. Diéguez, J. Íñiguez, N. Choudhury, L. Bellaiche, *Phys. Rev. Lett.* **2013**, *110* 187601.
- [37] Y.-W. Chen, J.-L. Kuo, K.-H. Chew, *J. Appl. Phys.* **2017**, *122*, 7 075103.
- [38] J. P. Allen, G. W. Watson, *Phys. Chem. Chem. Phys.* **2014**, *16* 21016.
- [39] R. A. Marcus, N. Sutin, *Biochimica et Biophysica Acta (BBA)-Reviews on Bioenergetics* **1985**, *811*, 3 265.
- [40] Newton, Marshall D., *Int. J. Quantum Chem.* **1980**, *18*, S14 363–391.
- [41] J. M. Moreau, C. Michel, R. Gerson, W. J. James, *Journal of Physics and Chemistry of Solids* **1971**, *32*, 6 1315 .
- [42] F. J. Morin, *Phys. Rev.* **1951**, *83* 1005.
- [43] H. J. Van Daal, A. J. Bosman, *Phys. Rev.* **1967**, *158* 736.
- [44] B. Zhao, T. C. Kaspar, T. C. Droubay, J. McCloy, M. E. Bowden, V. Shutthanandan, S. M. Heald, S. A. Chambers, *Phys. Rev. B* **2011**, *84* 245325.
- [45] F. Ramirez, E. Marinho Jr, C. Leão, J. Souza, *Journal of Alloys and Compounds* **2017**, *720* 47.
- [46] S. C. Das, S. Katiyal, T. Shripathi, *Journal of Applied Physics* **2018**, *124*, 17.
- [47] J. Kolte, P. H. Salame, A. Daryapurkar, P. Gopalan, *AIP Advances* **2015**, *5*, 9.
- [48] A. Perejón, N. Masó, A. R. West, P. E. Sánchez-Jiménez, R. Poyato, J. M. Criado, L. A. Pérez-Maqueda, *Journal of the American Ceramic Society* **2013**, *96*, 4 1220.
- [49] L. Pintilie, C. Dragoi, Y. Chu, L. Martin, R. Ramesh, M. Alexe, *Applied Physics Letters* **2009**, *94*, 23.
- [50] Y. Yao, W. Liu, C. L. Mak, *Journal of alloys and compounds* **2012**, *527* 157.
- [51] K. Momma, F. Izumi, *J. Appl. Crystallogr.* **2011**, *44*, 6 1272.

Energy barriers for small electron polaron hopping in bismuth ferrite from first principles

Supporting Information

Sabine Körbel*

Institute of Physical Chemistry and Institute of Condensed Matter Theory and Optics, Friedrich Schiller University, Fürstengraben 1, 07743 Jena, Germany

Email Address: skoerbel@uni-muenster.de

Keywords: *polarons, ferroelectrics, domain walls, density-functional theory, electronic transport*

1 Energy barriers for all hops at the 71° domain wall

Table 1: All computed 2NN energy barriers E_a in meV (maximal, for hop to, for hop fro) for small electron polaron hopping at 71° domain walls in BiFeO₃ for different strains.

strain ε	2NN hop	max. barrier	barrier \rightarrow	barrier \leftarrow	along
-0.17%	1''' \leftrightarrow 1''	26.0288	26.0288	25.9632	<i>t</i>
-0.17%	1''' \leftrightarrow 0''	35.1826	21.7337	35.1826	<i>s, r, t</i>
-0.17%	1''' \leftrightarrow 2'	45.2958	45.2958	5.72441	<i>s, r, t</i>
-0.17%	0 \leftrightarrow 1	28.8213	28.8213	14.9867	<i>s, r, t</i>
-0.17%	0 \leftrightarrow -1	54.3158	54.3158	8.43113	<i>s, r, t</i>
-0.17%	0 \leftrightarrow -1'	52.3914	52.3914	6.57196	<i>s, r, t</i>
-0.17%	0 \leftrightarrow -2	57.8417	57.8417	4.39795	<i>s</i>
-0.17%	0 \leftrightarrow 1'	27.9757	27.9757	14.1251	<i>s, r, t</i>
-0.17%	0 \leftrightarrow 0'	16.1782	16.1646	16.1782	<i>t</i>
-0.17%	0 \leftrightarrow 2	56.1503	56.1503	3.978	<i>s</i>
0%	1''' \leftrightarrow 1''	26.4468	26.4468	26.2967	<i>t</i>
0%	1''' \leftrightarrow 0''	37.3722	24.1059	37.3722	<i>s, r, t</i>
0%	1''' \leftrightarrow 2'	45.8927	45.8927	3.98957	<i>s, r, t</i>
0%	0 \leftrightarrow 1	27.8498	27.8498	14.1457	<i>s, r, t</i>
0%	0 \leftrightarrow -1	57.855	57.855	7.8752	<i>s, r, t</i>
0%	0 \leftrightarrow -1'	57.5892	57.5892	7.53427	<i>s, r, t</i>
0%	0 \leftrightarrow -2	65.2156	65.2156	9.67021	<i>s</i>
0%	0 \leftrightarrow 1'	29.808	29.808	16.0601	<i>s, r, t</i>
0%	0 \leftrightarrow 0'	25.4104	25.4104	25.2416	<i>t</i>
0%	0 \leftrightarrow 2	58.3416	58.3416	4.04886	<i>s</i>
0.34%	1''' \leftrightarrow 1''	28.7306	28.7306	28.7306	<i>t</i>
0.34%	1''' \leftrightarrow 0''	37.3883	24.9583	37.3883	<i>s, r, t</i>
0.34%	1''' \leftrightarrow 2'	49.2408	49.2408	3.27044	<i>s, r, t</i>
0.34%	0 \leftrightarrow 1	31.236	31.236	17.2023	<i>s, r, t</i>
0.34%	0 \leftrightarrow -1	64.0305	64.0305	6.62886	<i>s, r, t</i>
0.34%	0 \leftrightarrow -1'	64.1048	64.1048	6.86245	<i>s, r, t</i>
0.34%	0 \leftrightarrow -2	68.3597	68.3597	9.68162	<i>s</i>
0.34%	0 \leftrightarrow 1'	31.2503	31.2503	18.2218	<i>s, r, t</i>
0.34%	0 \leftrightarrow 0'	27.2722	27.2722	27.0263	<i>t</i>
0.34%	0 \leftrightarrow 2	61.1514	61.1514	3.40115	<i>s</i>

arXiv:2503.04394v1 [cond-mat.mtrl-sci] 6 Mar 2025

Table 2: All computed NN energy barriers E_a in meV (maximal, for hop to, for hop fro) for small electron polaron hopping at 71° domain walls in BiFeO_3 for different strains.

strain ε	NN hop	max. barrier	barrier \rightarrow	barrier \leftarrow
-0.17%	$1''' \leftrightarrow 1$	15.5868	15.5868	14.2278
-0.17%	$1''' \leftrightarrow 0$	28.4327	15.957	28.4327
-0.17%	$1''' \leftrightarrow 2$	43.2275	43.2275	3.53078
-0.17%	$0 \leftrightarrow 1''$	20.5007	20.5007	7.95949
-0.17%	$0 \leftrightarrow 0''$	31.1105	30.1372	31.1105
-0.17%	$0 \leftrightarrow -1'''$	49.7103	49.7103	3.24223
0%	$1''' \leftrightarrow 1$	15.0761	15.0761	13.7343
0%	$1''' \leftrightarrow 0$	28.3443	15.9821	28.3443
0%	$1''' \leftrightarrow 2$	45.3943	45.3943	3.4638
0%	$0 \leftrightarrow 1''$	21.3654	21.3654	8.85306
0%	$0 \leftrightarrow 0''$	32.3591	31.4551	32.3591
0%	$0 \leftrightarrow -1'''$	54.5359	54.5359	3.87857
0.34%	$1''' \leftrightarrow 1$	16.3716	16.3716	13.8598
0.34%	$1''' \leftrightarrow 0$	28.0379	16.516	28.0379
0.34%	$1''' \leftrightarrow 2$	48.9629	48.9629	2.7345
0.34%	$0 \leftrightarrow 1''$	24.2071	24.2071	12.6755
0.34%	$0 \leftrightarrow 0''$	34.6276	33.7195	34.6276
0.34%	$0 \leftrightarrow -1'''$	62.1718	62.1718	4.09336

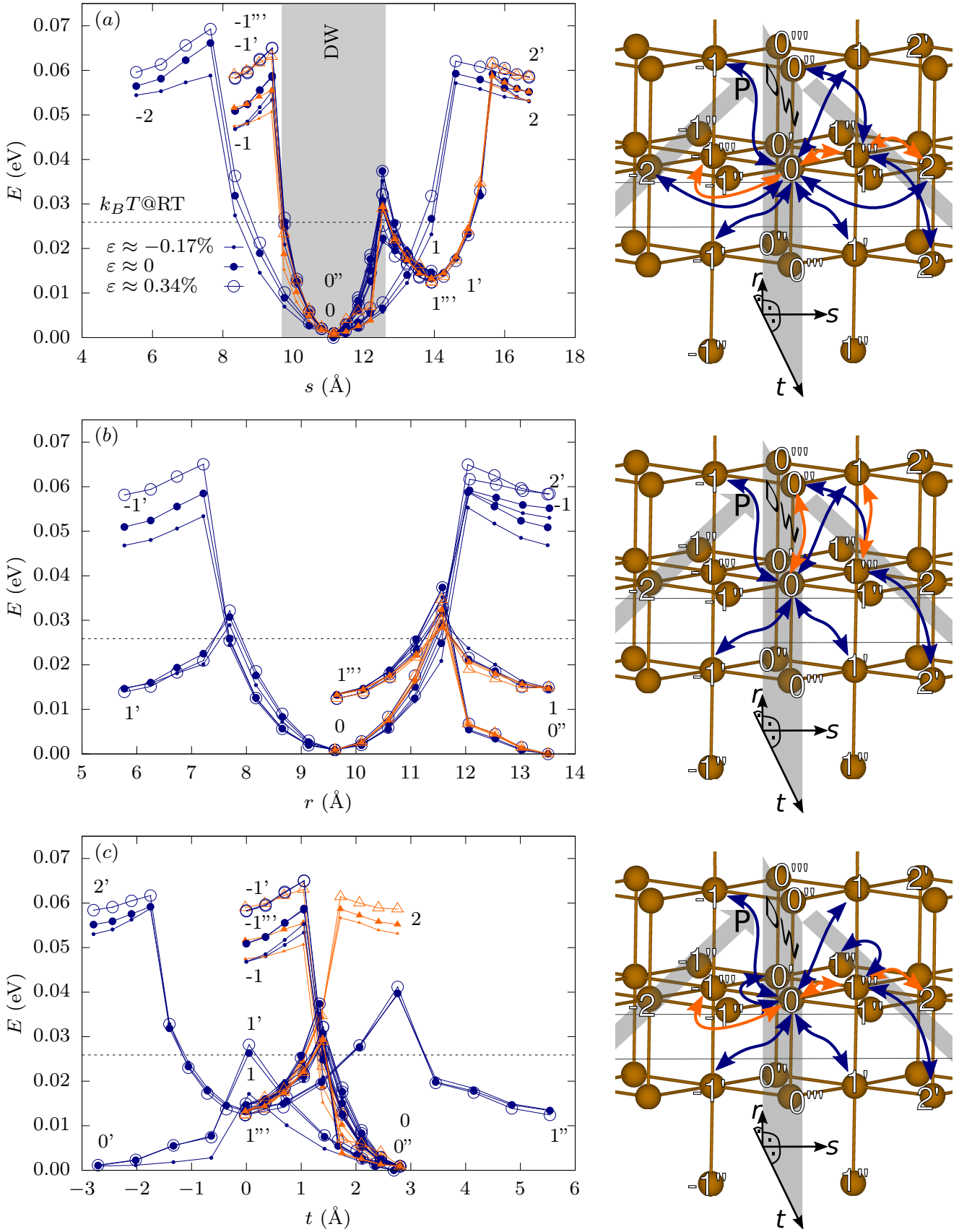


Figure 1: Energy barriers of polaron hops at the 71° domain wall. (a) All hops with a component across the wall, (b) and (c): all hops with components along the wall. Orange triangles: nearest-neighbor, dark-blue circles: second-nearest-neighbor hops. Numbers indicate the Fe positions on the right and in Figure 2(b) in the main text. Hop directions were projected on (a) the s coordinate, (b) the r coordinate, and (c) the t coordinate.

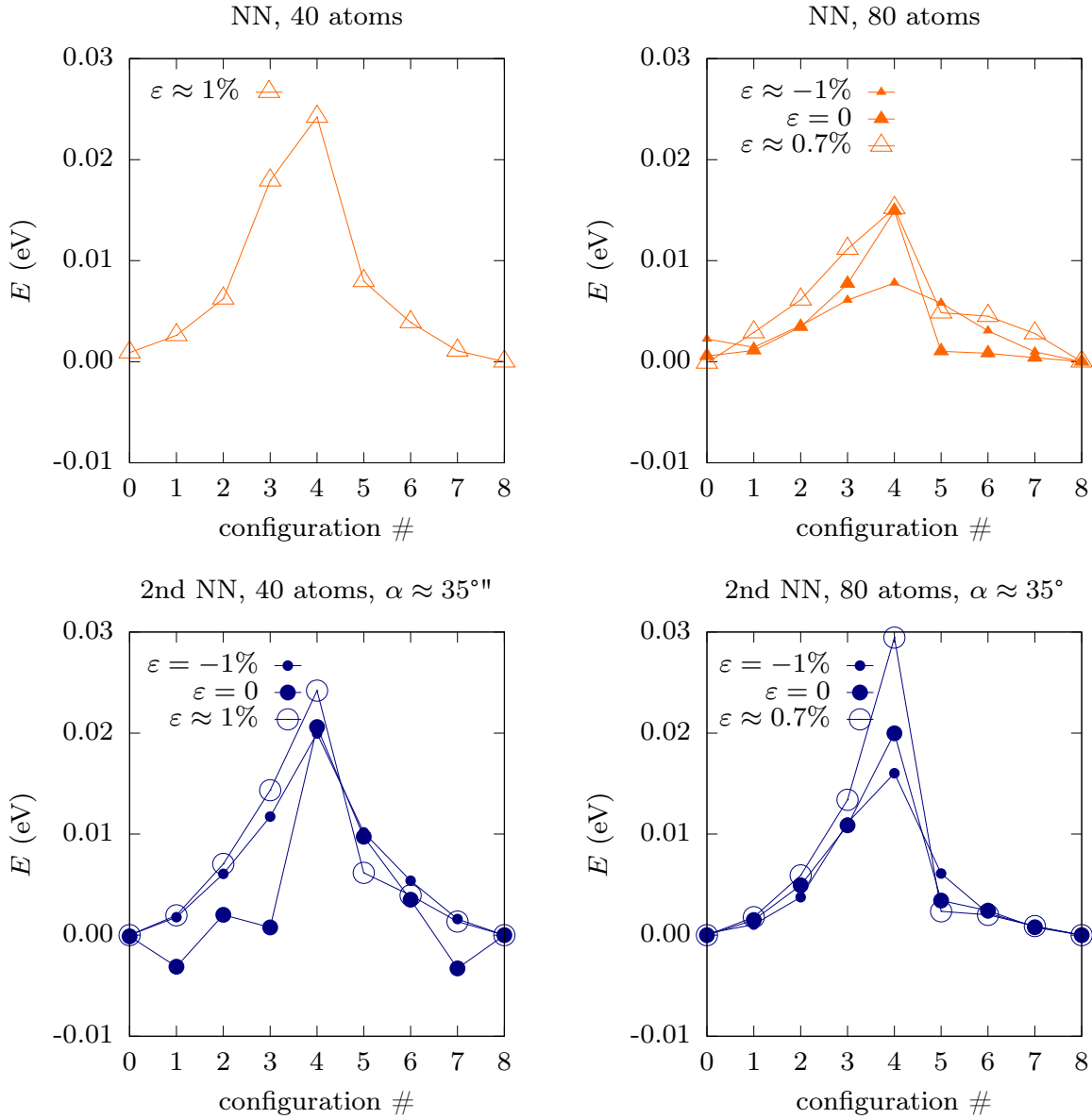


Figure 2: Energy barriers for polaron hopping between NN and 2NN sites for supercells with 40 atoms (left) and 80 atoms (right) with different lattice strain ε .

2 Convergence of energy barriers with respect to supercell size

Barriers in bulk were calculated in supercells with 40 and with 80 atoms, respectively. Figure 2 shows hopping barriers in bulk for different supercell sizes (40 and 80 atoms). For both supercell sizes, the barriers are close to the thermal energy at room temperature. The similar results obtained with different supercell sizes indicate that convergence with respect to supercell size was approximately achieved.

The strain reference (zero strain, $\varepsilon = 0$) corresponds to the optimized geometry of bulk without excess electron. Tensile strain, $\varepsilon > 0$, corresponds to the optimized geometry of bulk with excess electron.